Electronic Supplementary Material (ESI) for Energy & Environmental Science
This journal is © The Royal Society of Chemistry 2013

Synthesis, Photoelectrochemical Properties, and First Principle Study of n-type $CuW_{1-x}Mo_xO_4$ Electrodes Showing Enhanced Visible Light Absorption

James C. Hill,[a] Yuan Ping,[b] Giulia A. Galli,[b,] and Kyoung-Shin Choi[c,]**

[a]Department of Chemistry, Purdue University, West Lafayette, IN 47907.

[b]Department of Chemistry, University of California, Davis, CA 95616.

[c]Department of Chemistry, University of Wisconsin-Madison, Madison, WI 53706.

Supporting Information

* Correspondence and requests for materials should be addressed to K.-S. Choi (e-mail: kschoi@chem.wisc.edu) and G.A. Galli (e-mail: gagalli@ucdavis.edu).

Experimental Details

Synthesis. The plating solution was prepared by dissolving $Na_2WO_4 \cdot 2H_2O$ in water (40 mM). Then dilute nitric acid was added to lower the solution pH from 9 to 4 before adding $Cu(NO_3)_2 \cdot 3H_2O$ (final concentration: 40 mM). Otherwise, a green precipitate would form upon the addition of $Cu(NO_3)_2 \cdot 3H_2O$, which is most likely $CuWO_4 \cdot 2H_2O$.[24-25] After the addition of $Cu(NO_3)_2 \cdot 3H_2O$, the solution pH was adjusted to 2.75 and the solution was heated to 70 °C before *p*-benzoquinone (final concentration: 50 mM) was added.

Electrodeposition was performed in an undivided cell using an Ag/AgCl (4 M KCl) reference electrode, a glass slide sputter coated with 1000 Å of platinum atop 300 Å of titanium as the counter electrode, and fluorine-doped tin oxide (FTO) (8-12 Ω resistance, area of 2 cm^2) as the working electrode. A VMP2 multi-channel potentiostat (Princeton Applied Research) was used for all electrodepositions. A constant potential of -0.1 V vs. Ag/AgCl (4 M KCl) was applied to reduce benzoquinone until 0.72 C/cm^2 of charge was passed. The average deposition current ranged from 2.5 mA/cm^2 to 3.1 mA/cm^2 and the average deposition time ranged from 230 s to 290 s.

All as-deposited films were amorphous and were converted to crystalline $CuWO_4$ and $CuW_{1-x}Mo_xO_4$ electrodes by annealing at 500 °C in the air for 1 hour (ramping rate, 2 °C/min).

Characterization. Powder x-ray diffraction (XRD) data was collected using a Scintag X2 or Bruker D8 diffractometer (Cu K_α radiation). Absorbance was measured with a Cary 5000 UV-visible light spectrophotometer. Scanning electron microscopy (SEM) images and energy dispersive spectroscopy (EDS) data were acquired via a field emission scanning electron microscope (FEI Nova NanoSEM) equipped with an EDS detector. Prior to imaging the samples were coated with *ca.* 2 nm thick Pt by a thermal evaporator to reduce charging and imaged at an accelerating voltage of 5 kV. The ratios obtained from EDS were collected at an accelerating voltage of 20 kV and analyzed using an Oxford Inca system coupled to the FEI Nova NanoSEM. Capacitance measurements for Mott-Schottky plots were obtained using an EG&G Princeton Applied Research potentiostat (model 263A) linked with a Princeton Applied Research frequency response detector (FRD100). A sinusoidal modulation of 10 mV was applied at frequencies of 5 - 15 kHz.

Photocurrent Measurements. Photocurrent measurements were obtained with simulated solar illumination using a 300 W xenon arc lamp (Oriel) with intensity adjusted to 100 mW/cm^2 using a research radiometer (International Light, IL 1700) coupled with a thermopile detector (International Light, SED623/H/N/K15) by passing the beam through neutral density filters, an AM 1.5G filter, and a water filter. The beam passed through an optical fiber and illuminated 0.2 cm^2 of the sample through the FTO substrate (back-side illumination). A fused silica cell was used and the setup consisted of $CuWO_4$ or $CuW_{1-x}Mo_xO_4$ films as the working electrode, or photoanode, a glass slide sputter coated with 1000 Å of platinum on 300 Å of titanium as the counter electrode, and an Ag/AgCl reference electrode (4 M KCl). While all measurements were carried out using an Ag/AgCl (4M KCl) reference electrode, results in this study were presented against the reversible hydrogen electrode (RHE) for ease of comparison with the H_2 and O_2 redox levels and with other literature reports that used electrolytes with different pH conditions by converting the potential using the following equation.

$$E\ (\text{vs. RHE}) = E\ (\text{vs. Ag/AgCl}) + E_{Ag/AgCl}\ (\text{ref}) + 0.0591\ \text{V} \times \text{pH}$$

($E_{Ag/AgCl}$ (ref) = 0.1976 V vs. NHE at 25 ºC)

0.1 M phosphate buffer (pH 7) was used as the electrolyte. The phosphate buffer was prepared by dissolving 0.1 M NaH_2PO_4 in DI water and adjusting the pH to 7 with NaOH. Photocurrent density-potential curves were measured using a potential scan rate of 10 mV/s.

Incident photon-to-current conversion efficiency (IPCE) was determined using illumination from a 150 W Xe arc lamp passed through an AM 1.5G filter and neutral density filters to approximate the output of the sun. Monochromatic light was produced by an Oriel Cornerstone 130 monochromator with a 10 nm bandpass. The intensity of incident light was measured using a research radiometer (International Light, IL 1700) with a silicon photodiode detector (International Light, SED 033). IPCE was measured in 0.1 M phosphate buffer (pH 7) with the same three-electrode setup described above for photocurrent, using a Princeton Applied Research Potentiostat/Galvanostat model 263A to apply 1.0 V vs. Ag/AgCl (1.61 V vs. RHE).

Oxygen Detection. Oxygen measurements were performed using 400 mW/cm^2 illumination with an AM 1.5G filter to ensure a higher signal-to-noise ratio because O_2 generated from the illuminated area of the sample was not substantial when standard illumination (100 mW/cm^2, AM 1.5G) was used. A custom-built airtight split cell divided with a frit, 13 mm O.D. was used for all O_2 measurements. The split cell was made airtight by plastic caps with o-rings and copper rods inserted through the cap to attach the electrodes via copper adhesive tape. The oxygen sensor consisted of a platinum-porphyrin-based fluorescence sensor, FOSPOR-R 1/16" (Ocean Optics), inserted into the septum on the cap of the split cell. A two point calibration was performed using argon as 0% O_2 and air as 20.9% O_2. Both sides of the split cell were filled with 30 mL of electrolyte and had approximately 15 mL of headspace. The solution and headspace were purged with argon. The split cell was not completely airtight and slowly leaked air into the compartment. Therefore a leak rate was calculated and subtracted from the experimental data by determining the slope of the baseline before and after photoelectrochemical measurements were taken. The probe measured actual O_2 produced in mole percent, which was converted to micromoles of O_2 after accounting for O_2 dissolved in the electrolyte with Henry's Law. The theoretical amount of O_2 produced was determined by assuming the amount of charge passed during illumination corresponded to 100% Faradaic efficiency toward O_2 evolution. Thus the photocurrent-to-O_2 conversion efficiency was measured by the following equation (eq. 1)

$$\text{Photocurrent to } O_2 \text{ conversion efficiency (\%)} = \frac{\text{Actual amount of } O_2 \text{ detected}}{\text{Expected amount of } O_2 \text{ produced based on photocurrent}} \times 100\ \% \qquad (1)$$

Computational Details

We performed first-principles calculations within the framework of density functional theory (DFT) using the Quantum Espresso package[1] and different levels of theory (the spin polarized local density approximation (LDA), and the spin polarized generalized gradient approximation (GGA) using the PBE functional, and the LDA+U approximation. Our LDA results (Table 1 and 2) for the structural properties of $CuWO_4$ and $CuMoO_4$ are in good agreement with experimental lattice constants with errors within 2%, whereas PBE overestimates

the lattice constant by 2~3%. Therefore, in our band structure and projected density of state calculations (PDOS), we primarily used the LDA. The lattice constants of $CuWO_4$ and $CuMoO_4$ optimized in the paramagnetic state have larger errors compared with experiments (3~4%) than the ones optimized with anti-ferromagnetic ordering, consistent with the anti-ferromagnetic nature of $CuWO_4$ and $CuMoO_4$(III) found experimentally at low temperature. We used the lattice constants and geometries optimized with anti-ferromagnetic ordering in all calculations presented here, unless specified. The high symmetry points in the band structure plots are obtained from the online Bilbao Crystallographic Server[2] with space group $\bar{P}$, because $CuWO_4$ and $CuMoO_4$ (III) lattices have triclinic $\bar{P}$ symmetry. Norm-conversing Hartwigsen-Goedecker-Hutter (HGH) type pseudopotentials[3] were used in our calculations, including the 5s (4s) and 5p (4p) electrons of W (Mo) within the valence electrons; a kinetic energy cutoff of 140 Ry was used for the PW basis set. A (6x6x6) Monkhorst-Pack k-point grid was used for self-consistent ground state calculations and a (9x9x9) Monkhorst-Pack k-point grid was used for PDOS calculations.

Table S1. Equilibrium lattice parameters (a_0, b_0, c_0) of $CuWO_4$. LDA denotes results carried out within the Local Density Approximation[8,9] and anti-ferromagnetic ordering; LDA/noAFM denotes results carried out within the LDA without anti-ferromagnetic ordering; "PBE" denotes results carried out with the PBE functional[10] and anti-ferromagnetic ordering, and "Exp1, Exp2, Exp3" denote experimental values from three different experimental papers[4-6]. β is the angle between the a and c axes, α is the angle between b and c, and γ is the angle between a and b.

Method	Lattice constants (Å)			Angles (°)		
	a_0	b_0	c_0	α	β	γ
LDA	4.614	5.751	4.855	92.12	92.05	84.49
LDA/noAF	4.529	5.636	4.890	90.33	90.51	88.91
PBE	4.807	5.981	4.909	91.94	93.30	81.74
PBE/noAF	4.815	6.038	4.942	92.77	94.37	80.27
Exp1[4]	4.7095	5.8451	4.8849	88.30	92.50	97.20
Exp2[5]	4.694	5.830	4.877	91.64	92.41	82.91
Exp3[6]	4.7026	5.8389	4.8784	91.677	92.469	82.80

Table S2. Equilibrium lattice parameters (a_0, b_0, c_0) of $CuMoO_4$. LDA denotes results carried out within the Local Density Approximation and anti-ferromagnetic ordering; LDA/noAFM denotes results carried out within the LDA without anti-ferromagnetic ordering; "PBE" denotes results carried out with the PBE functional[10] and anti-ferromagnetic ordering, and "Exp" denotes experimental values[7]. β is the angle between the a and c axes, α is the angle between b and c, and γ is the angle between a and b.

Method	Lattice constants (Å)			Angles (°)		
	a_0	b_0	c_0	α	β	γ
LDA	4.581	5.753	4.844	91.45	91.37	84.01
LDA/noAF	4.535	5.650	4.855	90.65	90.65	87.03
PBE	4.861	6.031	4.939	91.66	93.78	79.27
PBE/noAF	4.818	6.044	4.947	92.28	94.21	79.52
Exp[7]	4.7152	5.8399	4.8583	91.04	92.43	81.28

References

1. P. Giannozzi et al, *J. Phys. Cond. Matter.*, 2009, **21**, 395502.
2. M. I. Aroyo, A. Kirov, C. Capillas, J. M. Perez-Mato and H. Wondratschek, *Acta Crystallogr. A*, 2006, **62**, 115-128.
3. C. Hartwigsen, S. Goedecker and J. Hutter, *Phys. Rev. B*, 1998, **58**, 3641-3662.
4. L. Kihlborg, E. Gebert, *Acta Crystallogr. B*, 1970, **26**, 1020-1025.
5. J. B. Forsyth, C. Wilkinson and A. I. Zvyagin, *J. Phys.: Condens. Matter*, 1991, **3**, 8433.
6. J. Ruiz-Fuertes, D. Errandonea, A. Segura, F. J. Manjón, Z. Zhu and C. Y. Tu, *High Pres. Res.*, 2008, **28**, 565-570.
7. H. Ehrenberg, M. Wiesmann, J. Garcia-Jaca, H. Weitzel and H. Fuess, *J. Magn. Magn. Mater.*, 1998, **182**, 152-160.
8. W. Kohn and L. J. Sham, *Phys. Rev.*, 1965, **140**, A1133.
9. N. D. Mermin, *Phys. Rev.*, 1965, **137**, A1441.
10. J. P. Perdew, K. Burke and M. Ernzerhof, *Phys. Rev. Lett.*, 1996, **77**, 3865.

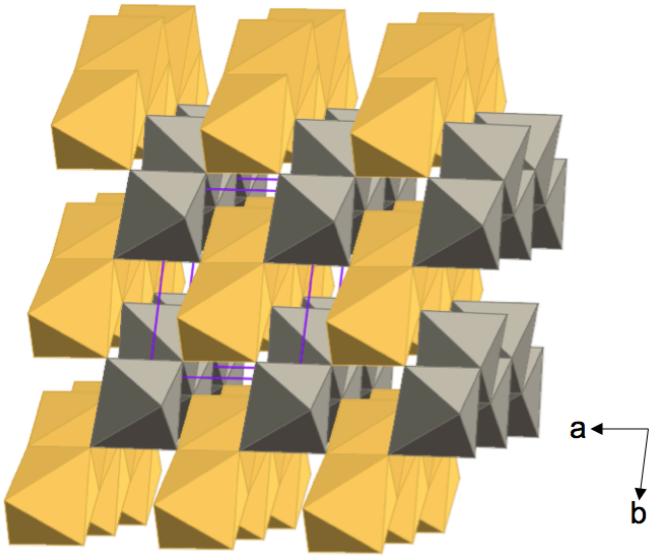

Figure S1. Wolframite structure of $CuWO_4$ showing the connectivity of Cu-centered (yellow) and W-centered (gray) octahedral.

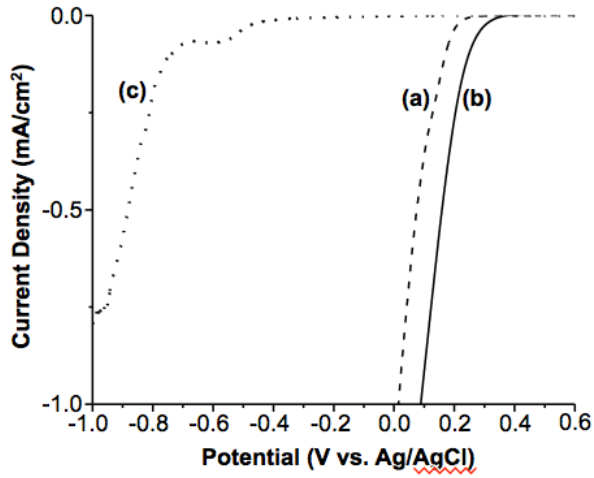

Figure S2. Linear sweep voltammograms (LSVs) obtained (a) in a solution containing 40 mM $Cu(NO_3)_2$ solution (pH 2.75) at 70 °C and (b) in a solution containing 40 mM $Cu(NO_3)$ and 50 mM *p*-benzoquinone (pH 2.75) at 70 °C. (c) LSV of nitrate reduction measured in 80 mM $NaNO_3$ (pH 2.75) at 70 °C is also shown for comparison. The results show that while the reduction of nitrate occurs at a more negative potential than the reduction of Cu^{2+}, the reduction of benzoquinone occurs at a more positive potential than the reduction of Cu^{2+} under the conditions used in this study.

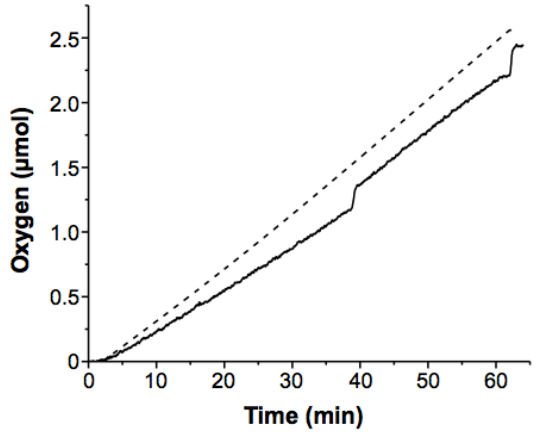

Figure S3. Oxygen detection during photocurrent measurement of a $CuW_{0.35}Mo_{0.65}O_4$ photoanode. O_2 detected by a fluorescence based sensor (---) is compared with O_2 calculated from charge passed (—) during a photocurrent measurement at 1.61 V vs. RHE (1.0 V vs. Ag/AgCl) in a 0.1 M sodium phosphate buffer (pH 7) assuming 100% Faradaic efficiency for O_2 production (Light intensity: 400 mW/cm^2 with an AM 1.5G filter). A few abrupt increases in O_2 amount in the measured data are due to the burst of large O_2 bubbles. This result shows that more than 90% of photocurrent was associated with O_2 evolution.

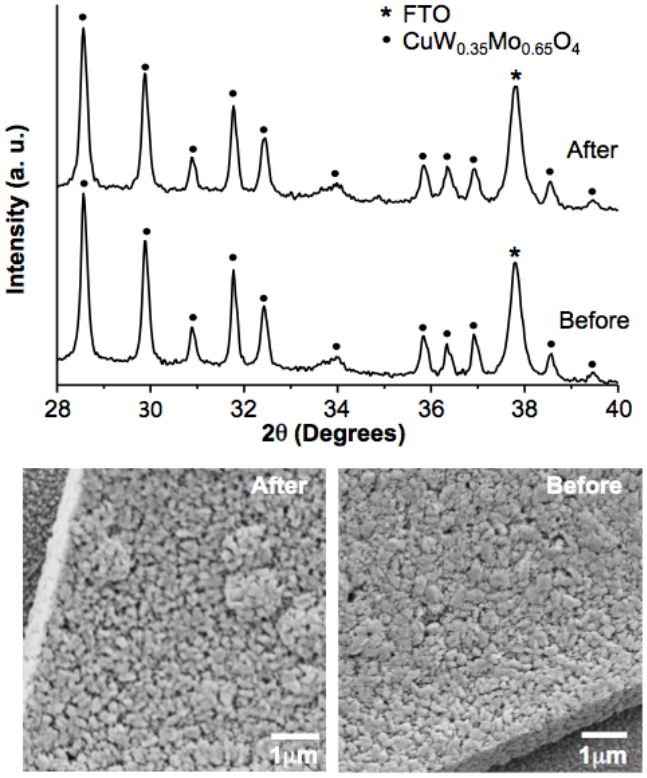

Figure S4. Comparison of XRD patterns (top) and SEM images (bottom) of a $CuW_{0.35}Mo_{0.65}O_4$ photoanode before and after a 30 minute photocurrent measurement. Photocurrent measurement conditions used in this experiment are identical to those used to generate photocurrent shown in Figure 3(b) in the main text.

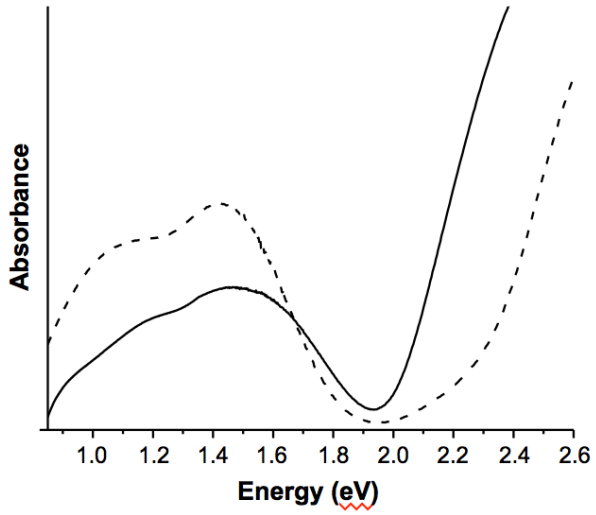

Figure S5. NIR-vis absorption spectra of $CuWO_4$ (dashed line) and $CuW_{0.35}Mo_{0.65}O_4$ (solid line) showing the absorption bands below the bandgap transition.

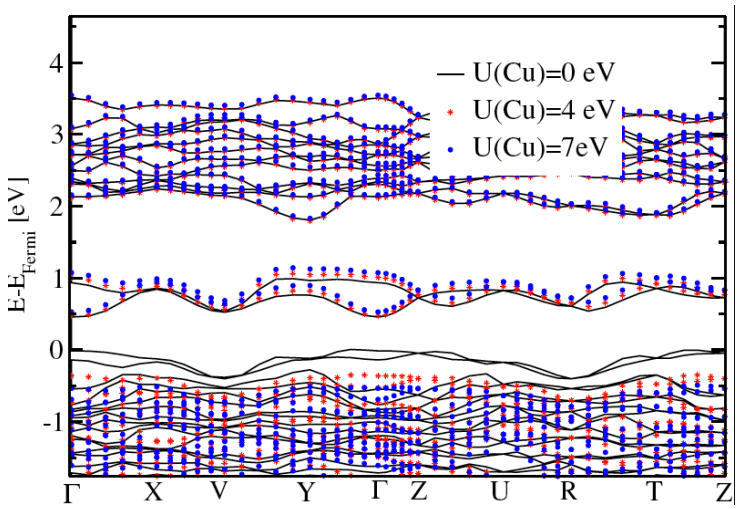

Figure S6. Band structure of Type-III $CuMoO_4$, aligned by Mo 4s,4p core states, as obtained from LDA and LDA+U calculations (at U= 0, 4, 7 eV, respectively).